Thermal Spray

Surface Engineering via Applied Research

8–11 May 2000

PROCEEDINGS OF THE 1st INTERNATIONAL THERMAL SPRAY CONFERENCE

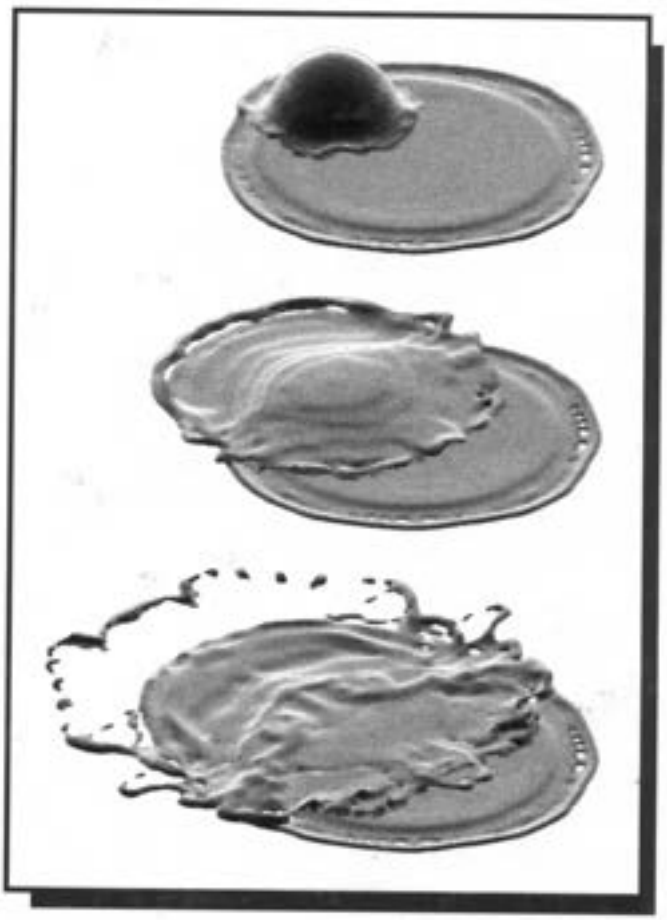

Edited by
Christopher C. Berndt

TSS
ASM Thermal Spray Society
An Affiliate Society of ASM International

DVS
German Welding Society
(Deutscher Verband für Schweisstechnik - DVS)

iiw iis
International Institute of Welding

Splat Formation in Off-Normal Angle Spray

H. Fukanuma, Y. Huang
Plasma Giken Co., Ltd., Toda City, Saitam, Japan

Introduction

The thermal spray process in an off-normal angle spray has been little studied. Several studies on microstructure and mechanical properties of off-normal angle spray deposits have been reported [1-3]. Montavon et al studied the splat morphology of off-normal angle spraying and showed that the elongation ratio increases from approximately 1 to 2 when the spray angle changes from 90° to 30°, and that the average splat area is little influenced by the spray angle [4, 5]. The elongation ratio is defined as the ratio of the longest distance "*a*" to the shortest distance "*b*". The length "*a*" and "*b*" are shown in Fig.1. Montavon and Coddet investigated the 3D profile of the splat sprayed at off-normal angles. They reported that the splat thickness profile is inclined and that a lower spray angle induces a higher slope in the splat thickness [6].

A few numerical studies have been reported very recently. Sobolev et al reported the relationship between the flattening characteristic and the Reynolds number at off-normal spray angles [7]. They calculated the splat radius under a certain velocity field in the splat and the assumption of splat circularity at spray angles between 90° to 45°. They showed that, as the spray angle decreases, the splat radius increases and the particle pressure on the substrate surface during flattening decreases. Our previous study proposed a mathematical model that predicted the elongation ratio as a function of the spray angle by introducing a parameter "*n*" that influences the ratio of the parallel velocity to the perpendicular velocity of the particle to the substrate. The model agreed with the experimental results at spray angles of 90° to 30° [8]. Bussmann et al reported the simulation results of off-angle impact by employing the RIPPLE method [9]. Nickel particle impact in plasma and HVOF sprays were simulated in the study.

The aim of the present study is to examine the splat shape at off-normal angles in plasma spray and to investigate the relationship between the splat elongation ratio and the spray angle on various spray materials and particle sizes. The applicability of the model to the experimental results is investigated.

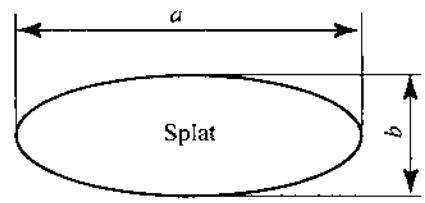

Fig. 1. The definition of the longest distance and shortest distance of a splat.

Experimental Procedure

In this study, six powders of aluminum, copper and nickel as metal spray materials, and alumina, titania and zirconia as oxide materials were sprayed, Table 1.

The substrate specimens were made of stainless steel. The dimensions of the specimen are shown in Fig. 2-a. The spray angle "φ" illustrated in Fig. 2-a was 90°, 75°, 60°, 45°, 30° and 15°. This is defined as the angle between the central axis of the torch and the surface plane of the specimen. Those six types of the specimen were arranged as shown in Fig. 2-b for plasma spraying.

In the study, the plasma spray torch was a SG-100 from Miller Thermal Company. The one-pass spray was made in the direction shown in Fig. 2-b. The spray parameters are listed in Table 2.

Table 1. Chemical composition and particle size range of the spray powder.

Material	Chemical Composition	Particle Distribution
Al	99% Al	< 106 μm
Cu	99.3% Cu	< 106 μm
Ni	99.8% Ni	45-105 μm
Al_2O_3	99% Al_2O_3	10~32 μm
TiO_2	99% TiO_2	10~45 μm
ZrO_2	93% ZrO_2, 4% CaO	5~45 μm

Table 2. Spray conditions for metals and oxides.

Parameter		Metal Material	Oxide Material
Arc Current		800 A	800 A
Arc Voltage		40 V	40 V
Arc Gas Flow	Ar	40 l/min.	40 l/min.
	He	20 l/min.	42.5 l/min.
Spray Distance		100 mm	100 mm
Torch Traverse Speed		800 mm/sec.	800 mm/sec.
Substrate Temperature		400 °C - 450 °C	

Results and Discussions

The shape of splats. Aluminum and alumina splats sprayed at angles of 90° to 15° are shown in Fig. 3 and 4, respectively, as typical examples. Figure. 3 shows that all aluminum splats have projections around peripheral regions at every spray angle. On the contrary, alumina splats have distinctive outlines, Fig. 4. Figures 3 and 4 show that splats of aluminum and alumina elongate as the spray angle decreases.

The profile of splats at an off-normal angle spray was found to be elliptic. Twenty splats of different materials that were sprayed at 75° to 15° were photographed and the lengths "*a*" and "*b*" of the splats shown Fig. 1 were measured from randomly selected photographs. The ellipse with the diameters that equate "*a*" and "*b*" of the splat was drawn on transparent paper and superimposed on the splat's photograph. Every splat was compared with the corresponding drawn ellipse. The results of nickel and zirconia splats are shown in Fig. 5. The elliptic contours are drawn with a dashed line in the figure. The figure shows that the splat profile fits its corresponding ellipse except for the peripheral projections around the splat. In particular, the contour lines of zirconia splats are clear. On the contrary the outlines of nickel splats are less distinct due to splashing in the downstream direction.

The relationship between "*a*" and "*b*". The long length and short length of splat "*a*" and "*b*" are defined as the major diameter and minor diameter of the ellipse, respectively, because splats can be characterized as an ellipse. Major diameter "*a*" and minor diameter "*b*" were measured on the splats of the six different materials at spray angles of 90° to 15°. Figures 6 shows that the relationship between the major diameter "*a*" and the minor diameter "*b*" of nickel splats is linear at every angle, 90° to 15°, and that the linear slope increases as spray angle decreases. Figure 7 and 8 show that aluminum and alumina have the same relationship as nickel.

The relationships between "*a*" and "*b*" of alumina, titania, zirconia and aluminum are illustrated in Fig. 9. The graph shows that these four different materials are nearly on the same line at each spray angle. Thus, the ratio "*a*/*b*" is not influenced by the chemistry of the materials. Figure 9 shows that "*a*" changes from around 50 μm to more than 1000 μm and "*b*" from less than 50 μm to around 400 μm. The linearity of the relationship between "*a*" and "*b*" holds over the wide range of splat sizes, that is, the ratio "*a*/*b*" does not depend on the splat size.

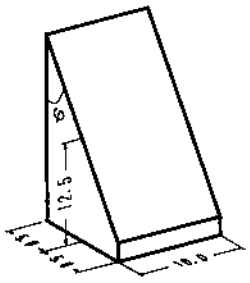

a. Specimen demensions

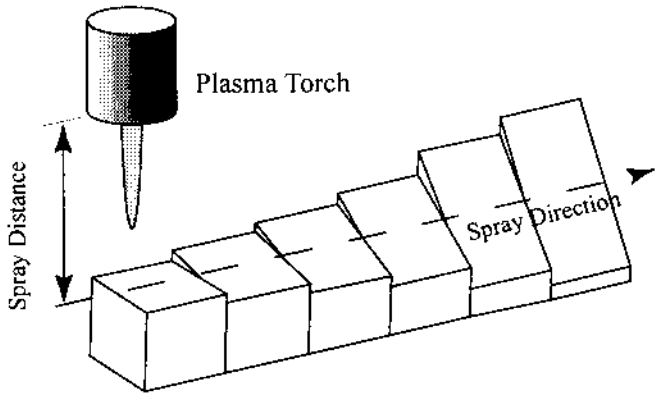

b. The specimem arramgement

Fig. 2. Specimen dimensions and arrangement for plasma spray.

The flattening process generally depends on the Reynolds number [10,11]. The Reynolds number is defined as:

$$\mathrm{Re} = \frac{\rho v_0 d_0}{\mu} \qquad (1)$$

Where ρ, v_0, d_0 and μ are the particle density, the velocity at impact, the diameter and viscosity, respectively. The flattened splat size is described as a function of the Reynolds number. The ratio "*a*/*b*" is independent on the splat size and implies it does not depend on the particle size, initial velocity and viscosity; that is, the ratio only depends on the spray angle.

The elongation ratio and the model. Montavon et al defined the ratio of "*a*" to "*b*' as the elongation ratio [4]. This term is also used to express "*a*/*b*" in this paper. Table 3 shows the experimental results as the average and standard deviation of the elongation ratio. The average elongation ratio increases as the spray angle decreases in all the materials. The standard deviation also rises as the spray angle is lowered. Each elongation ratio at 90° to 30° is very similar to the others; except at 15° as shown in Fig. 10.

The elongation ratio of copper is shown in Fig. 11 and that of titinia in Fig.12. The curves that were predicted by the

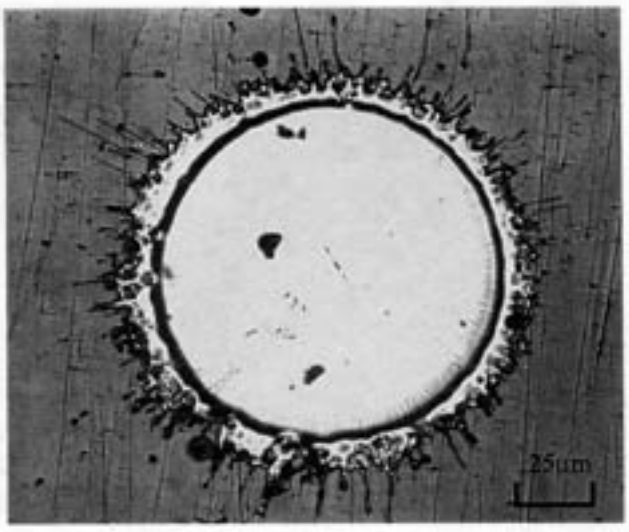

90°

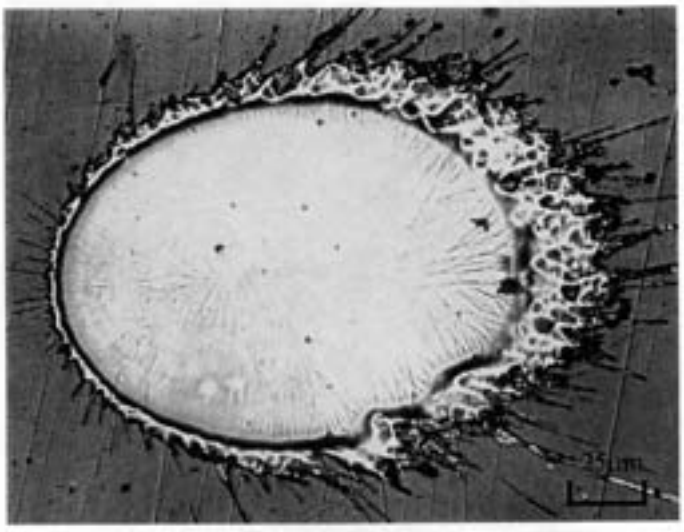

45°

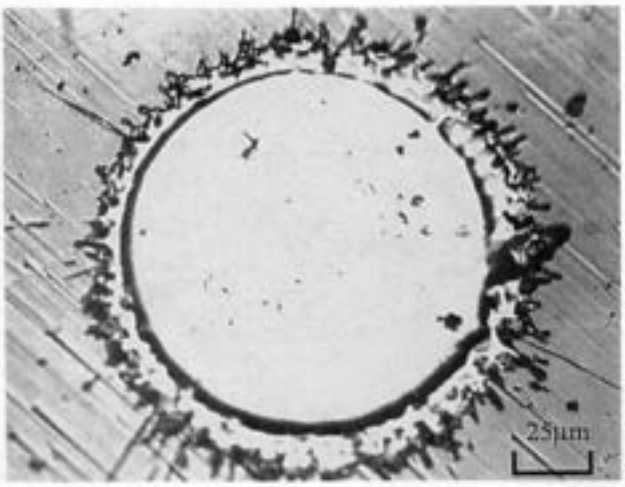

75°

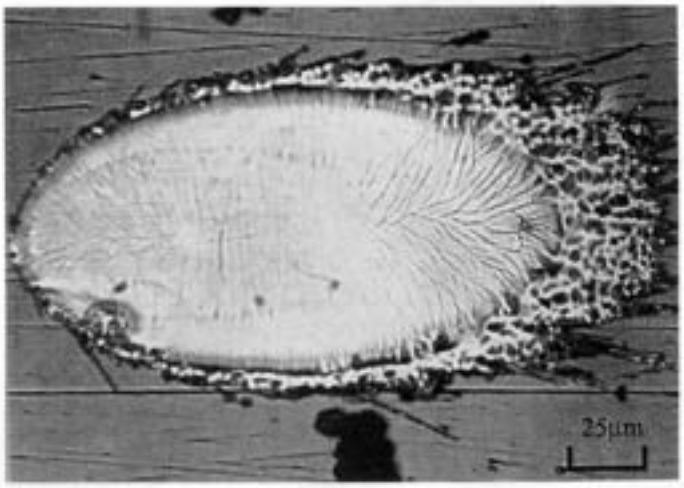

30°

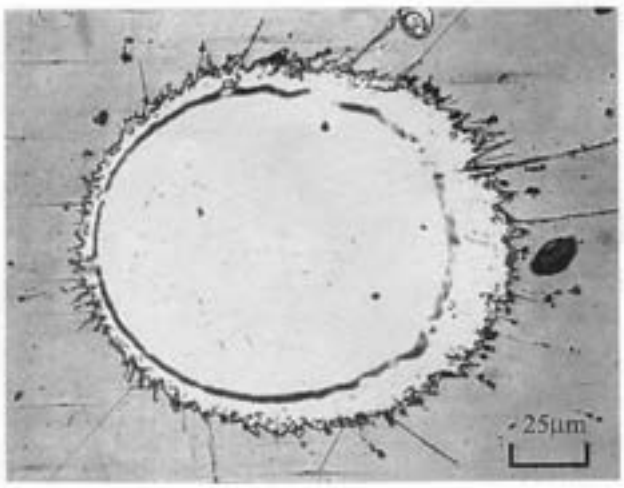

60°

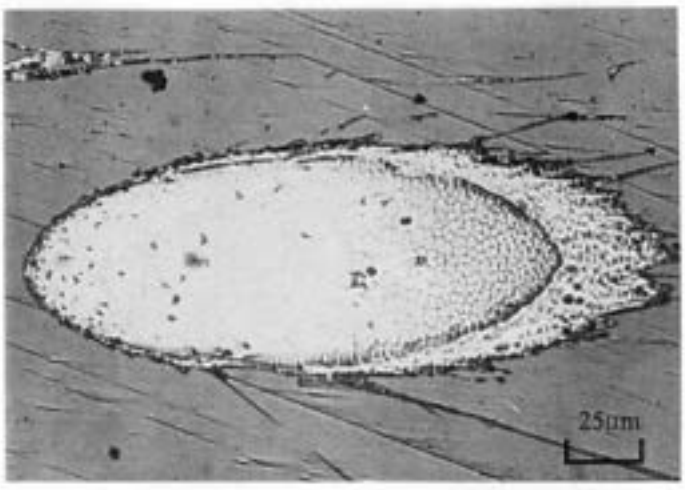

15°

Fig. 3. Aluminum splats sprayed at angles 90° to 15°.

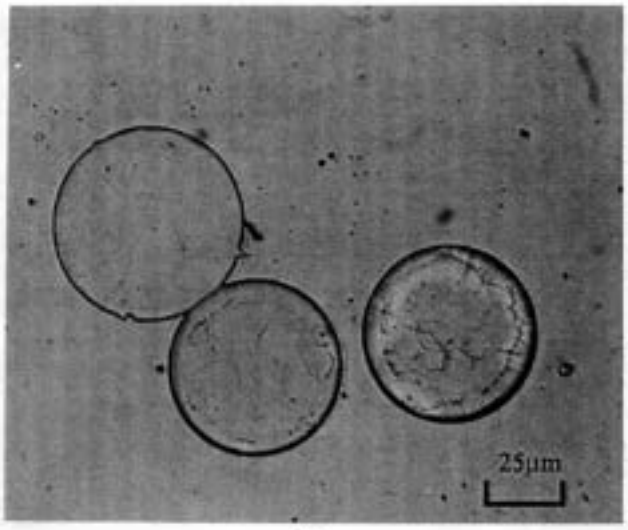

90°

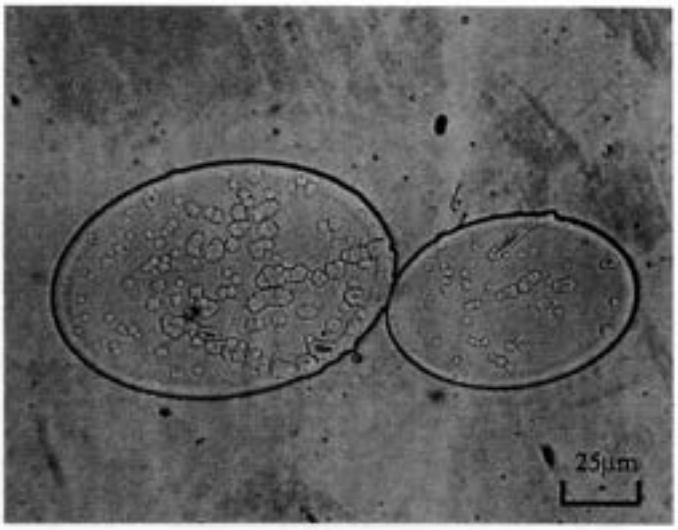

45°

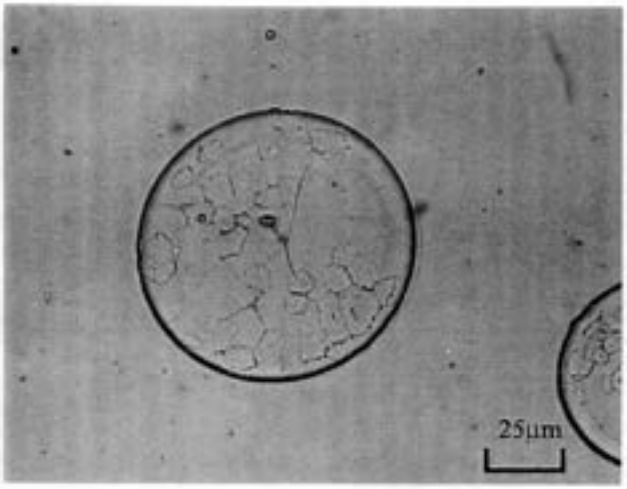

75°

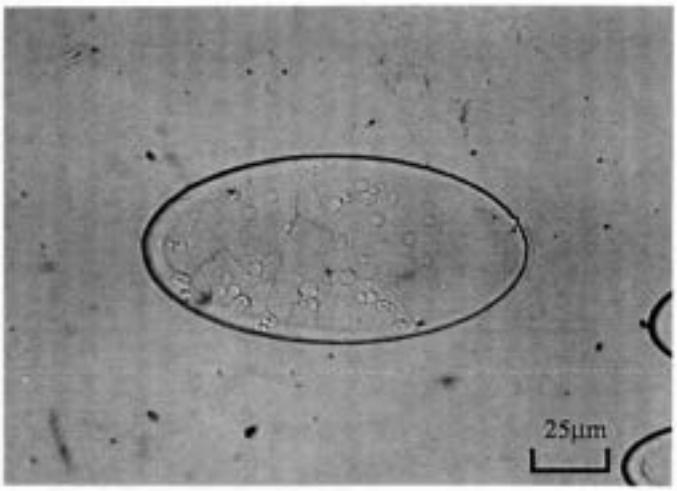

30°

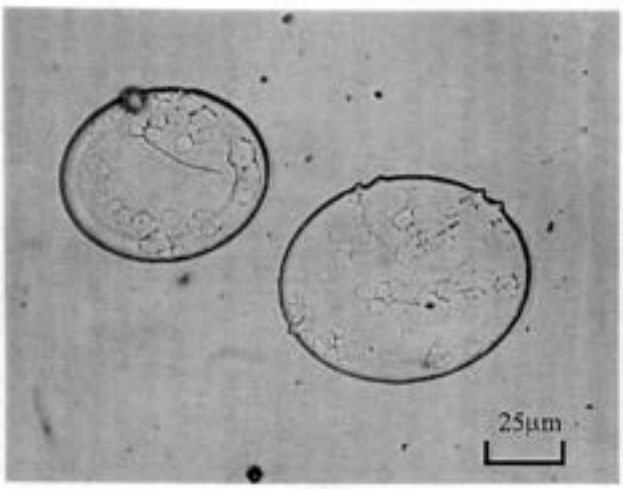

60°

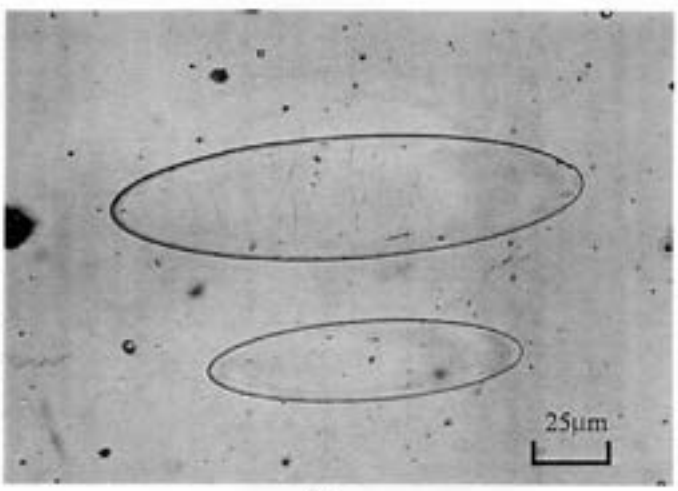

15°

Fig. 4. Alumina splats sprayed at angles 90° to 15°.

90°

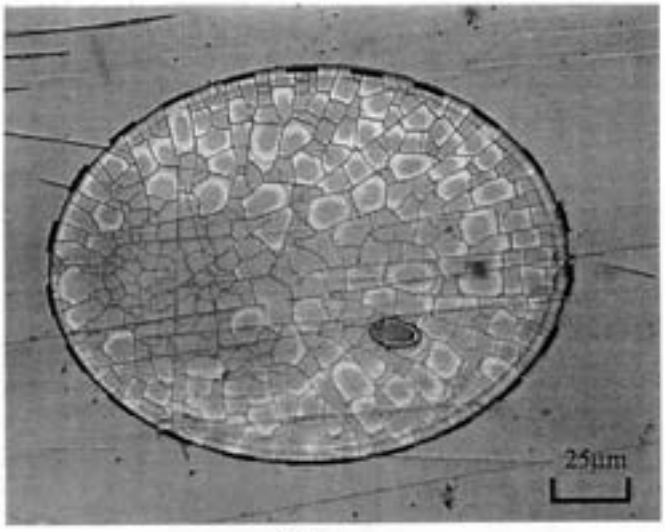

45°

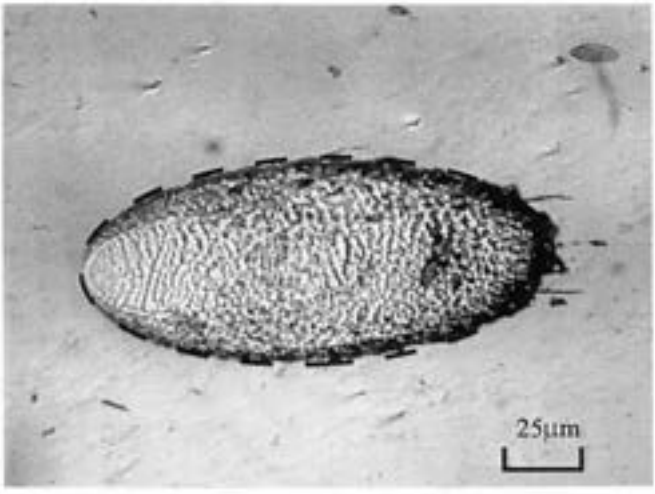

75°

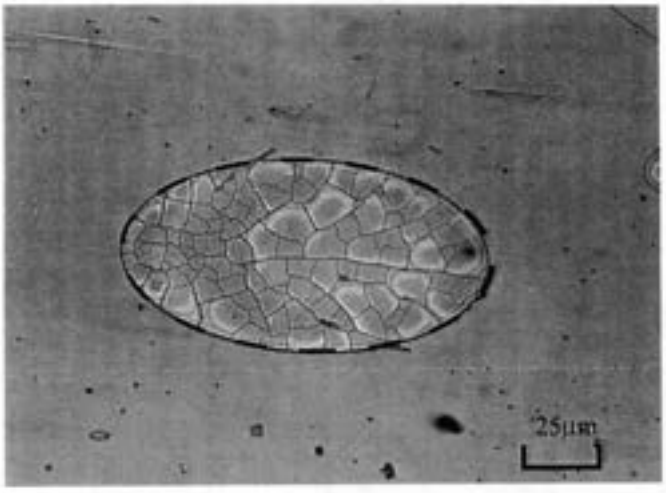

30°

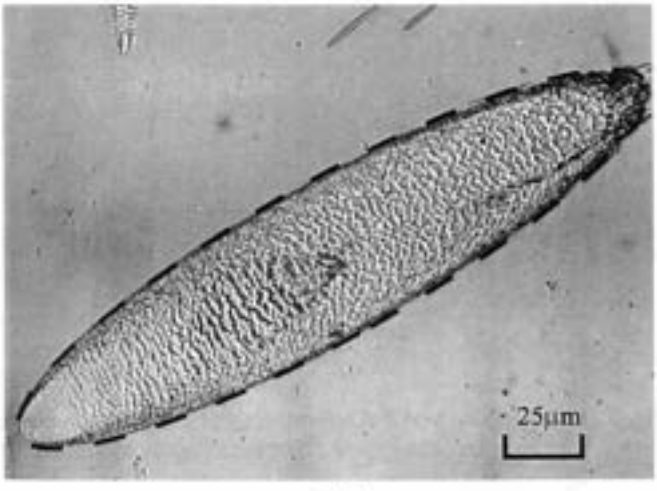

60°

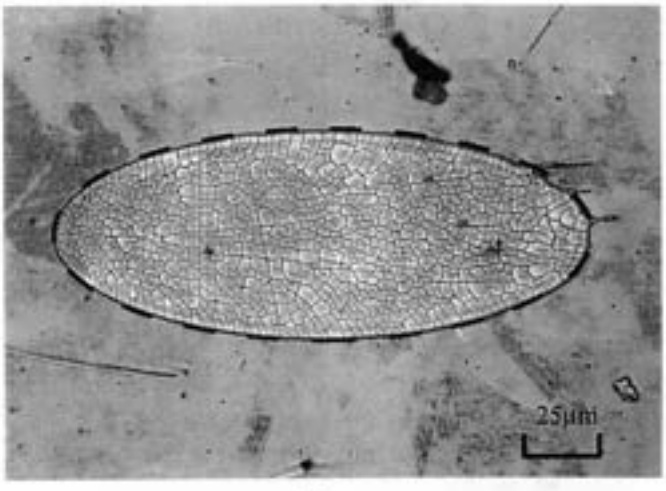

15°

Fig. 5. The comparison of nickel and zirconia splat shapes with elliptic contour..

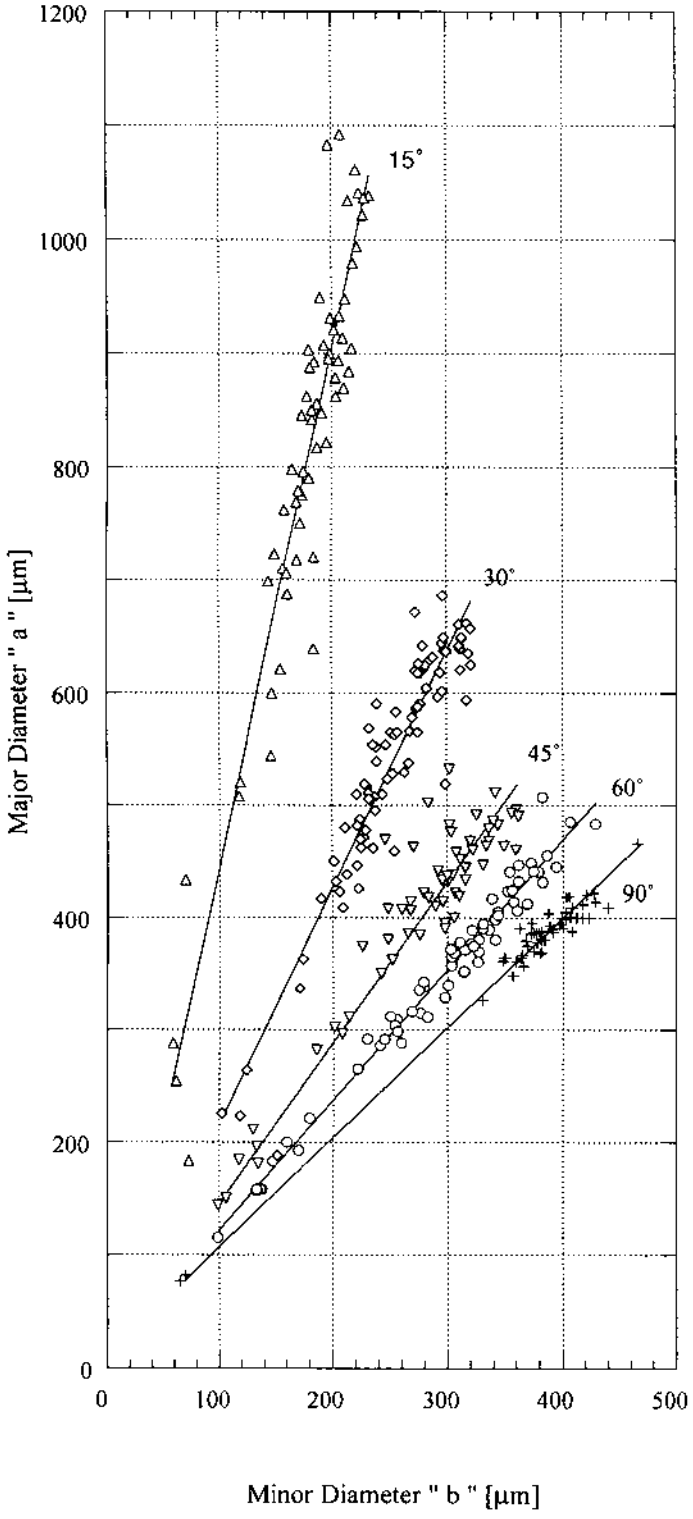

Fig. 6. The relationship of Nickel splat between the major diameter and the minor diameter at spray angles 90° to 15°.

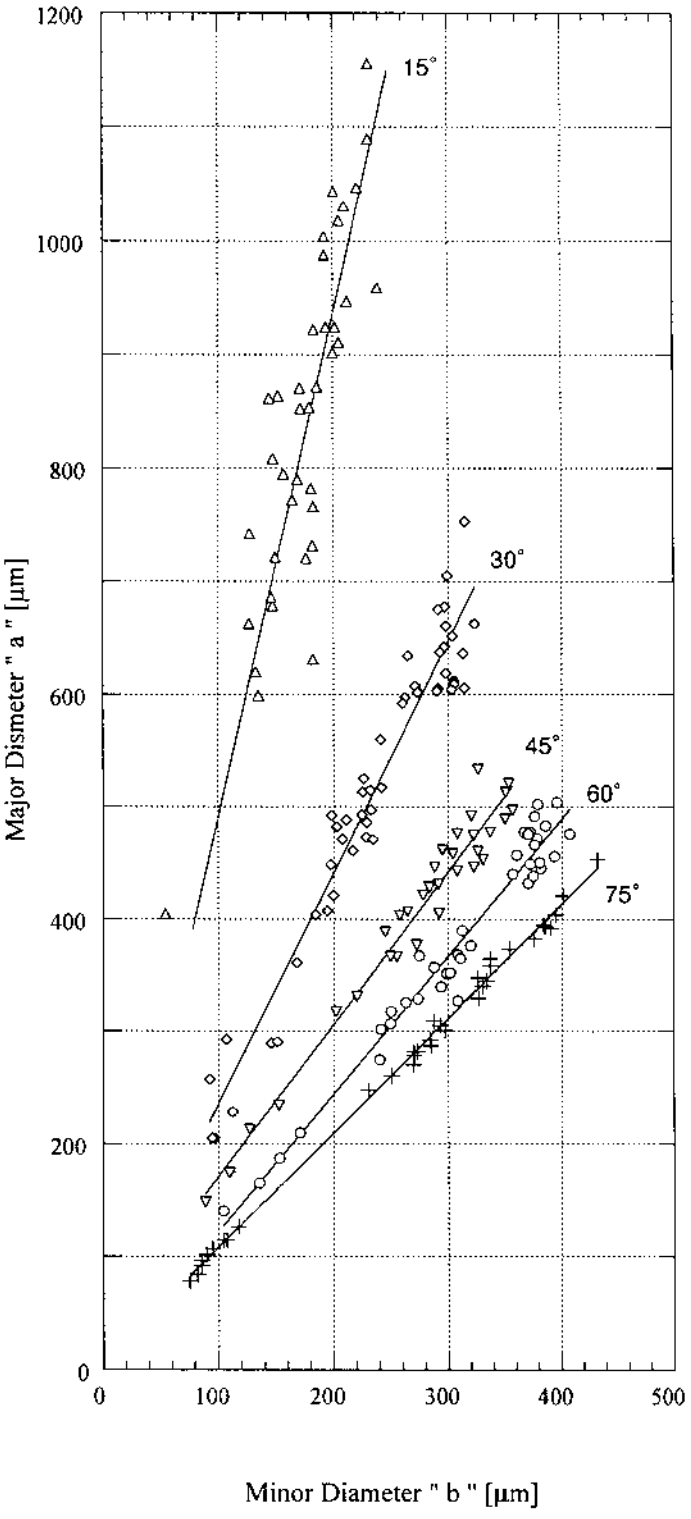

Fig. 7. The relationship of Aluminum splat between the major diameter and the minor diameter at spray angles 75° to 15°.

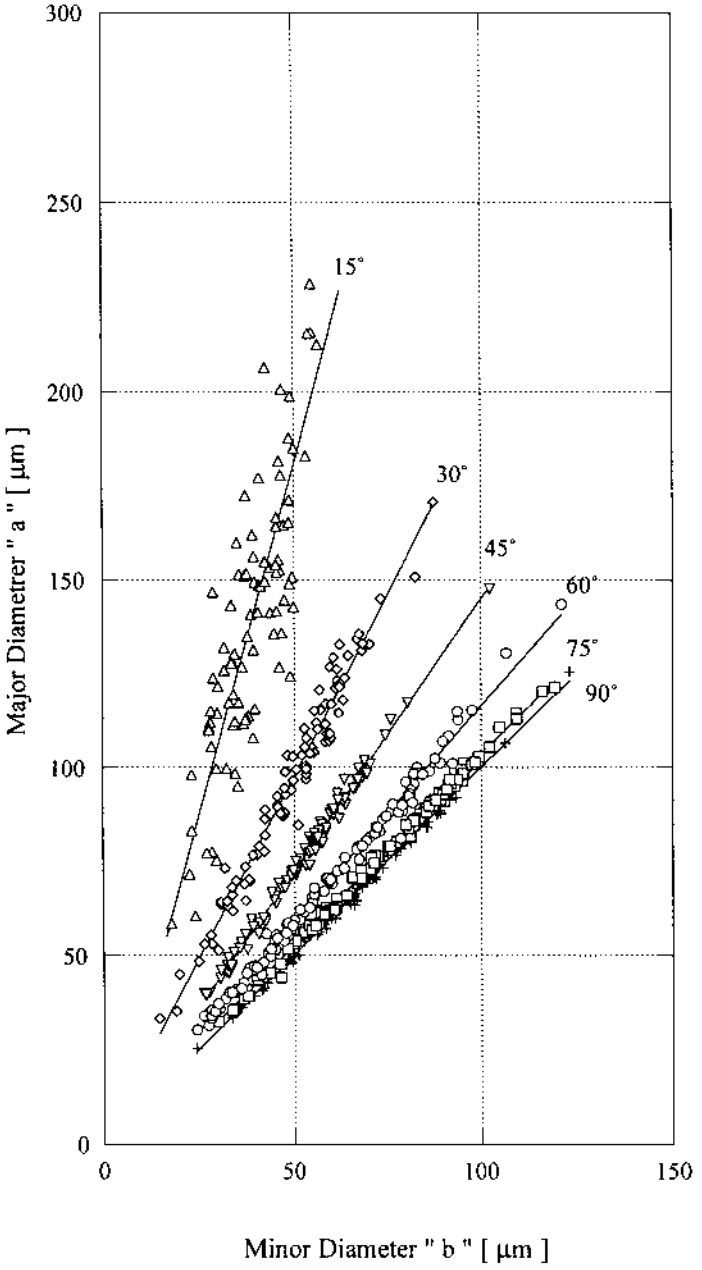

Fig. 8. The relationship of Alumina splat between the long diameter and the short diameter at spray angles 75° to 15° .

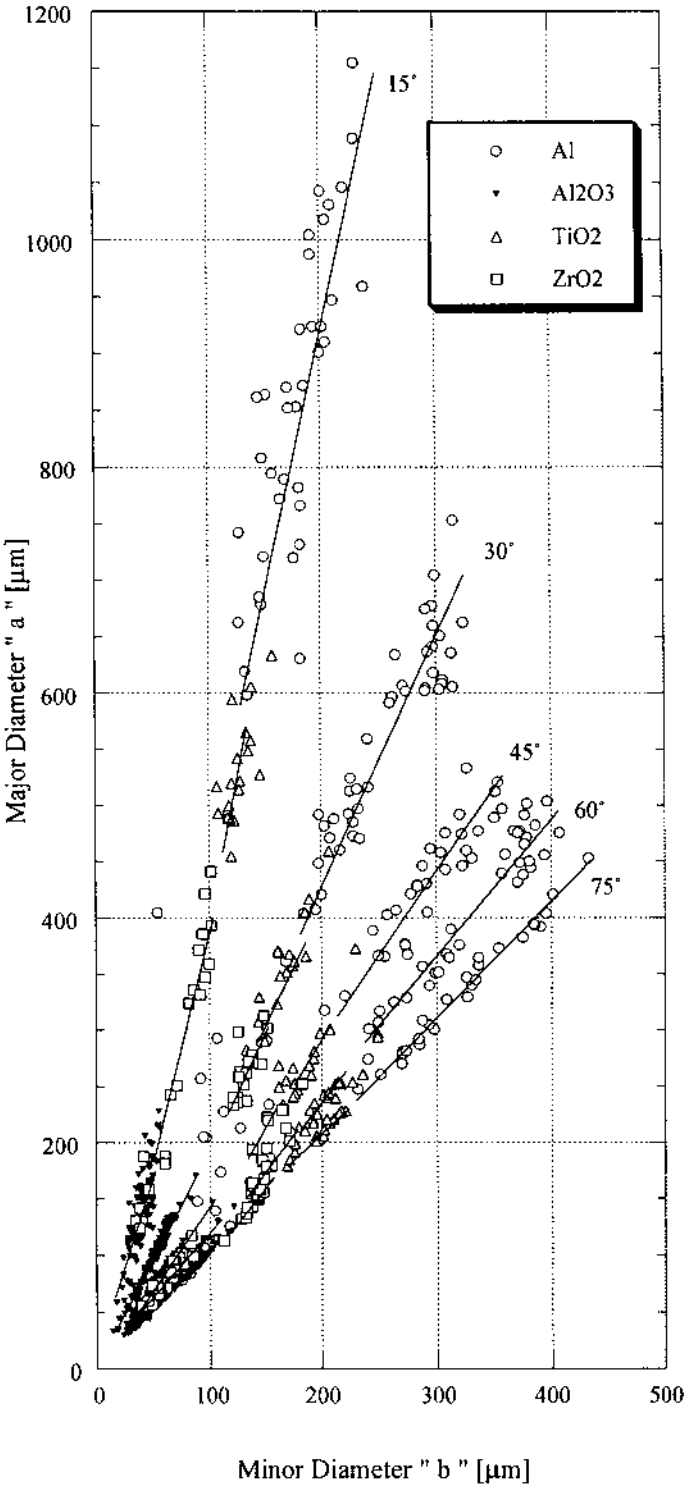

Fig. 9. The relationship between the long diameter and the short diameter at spray angles 75° to 15° .

Table 3. The average and standard deviation of the ratio "a/b" in the experimental results.

Material		Spray Angle φ					
		90°	75°	60°	45°	30°	15°
Nickel	Ratio Average	1.005	1.142	1.180	1.471	2.124	4.506
	Standard Deviation	0.046	0.060	0.044	0.121	0.166	0.482
	Sample Size	52	60	69	59	83	63
Copper	Ratio Average	1.002	1.124	1.157	1.458	2.046	5.459
	Standard Deviation	0.049	0.037	0.039	0.093	0.169	0.335
	Sample Size	10	25	13	21	17	24
Aluminum	Ratio Average	1.001	1.048	1.223	1.495	2.196	4.853
	Standard Deviation	0.038	0.033	0.061	0.084	0.177	0.665
	Sample Size	30	34	38	34	49	38
Alumina	Ratio Average	1.005	1.050	1.189	1.462	2.048	3.984
	Standard Deviation	0.018	0.029	0.048	0.082	0.173	0.759
	Sample Size	87	100	119	85	90	88
Titania	Ratio Average		1.063	1.172	1.435	2.133	4.196
	Standard Deviation		0.029	0.031	0.116	0.108	0.307
	Sample Size		16	15	20	16	19
Zirconia	Ratio Average		1.060	1.198	1.420	1.989	3.734
	Standard Deviation		0.041	0.050	0.148	0.138	0.419
	Sample Size		16	23	24	19	24

mathematical model proposed in our previous study are plotted in the graphs [8]. The model derived an expression that describes the elongation ratio ER as a function of the spray angle φ and a parameter n. The equation is expressed as:

$$ER = \frac{1}{\sqrt{1 - \dfrac{-1 + \sqrt{1 + 576n^4 \tan^4 \varphi}}{288n^4 \tan^4 \varphi}}} \qquad (2)$$

The model curve agrees well with the experimental results at spray angles from 90° to 30°; however the theoretical value at 15° is larger than the experimental value, shown Fig. 11 and 12. The drop in splat temperature during flattening may cause this large deviation of the model from the experimental results, because the model assumes that the flattening process is isothermal. The flattening time becomes longer as the spray angle is lowered due to a reduction in the perpendicular velocity with respect to the substrate, that is, splat temperature at a lower angle becomes lower. Lower temperature causes higher viscosity of the molten fluid. The model also assumes that the particle moves relatively faster in the parallel direction to the substrate than in the perpendicular direction. The parameter "n" expresses the degree of resistance for the particle to move in the parallel direction. When the particle viscosity become higher, the ratio of the parallel velocity to the perpendicular velocity may decrease, then the elongation ratio lowers. The change of the viscosity during flattening may affect the elongation ratio. If the viscosity maintains the initial value during splat formation, the ratio could become larger. This may be the reason why the theoretical value becomes larger than the experimental results.

Variation in the experimental results. The standard deviation of the experimental elongation ratio increases as the spray angle decreases; as shown in Table 3 and Fig. 10. This deviation of the experimental elongation ratio increases as the spray angle decreases; as shown in Table 3 and Fig. 10.

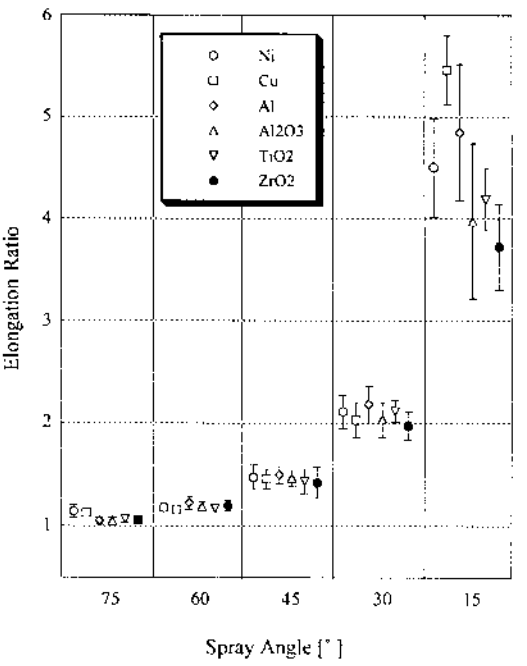

Fig. 10. The average and standard deviation of the elongation ratio at spray angles of 75° to 15° for all materials.

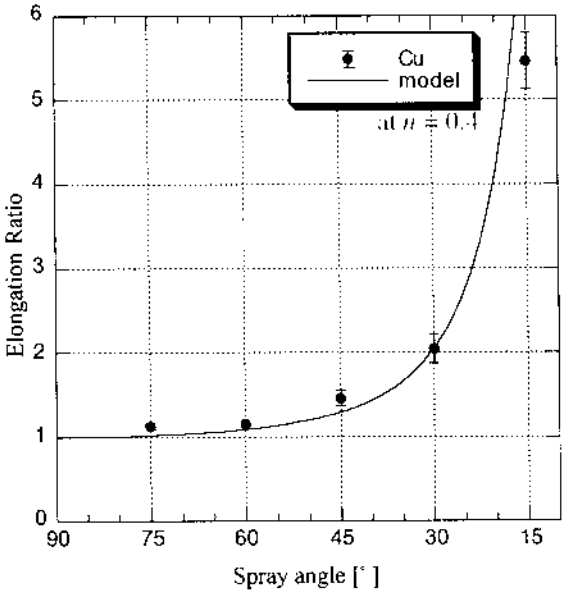

Fig. 11. The relationship between the elongation ratio and the spray angle in Copper spray, and the comparison of the model with experimental results.

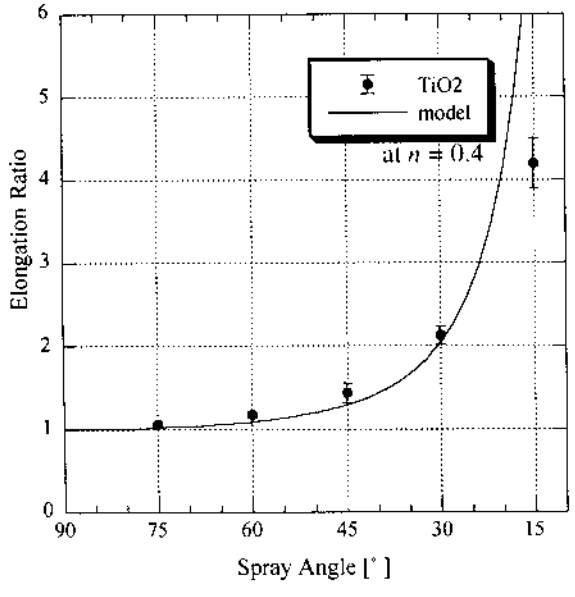

Fig. 11. The relationship between the elongation ratio and the spray angle in Titania spray, and the comparison of the model with experimental results.

This variation originates from broadening of the spray pattern. The particle stream from the plasma nozzle has a broadening angle, as shown in Fig. 13. The particle impact angle changes in the range ϕ to ψ. The difference between the maximum and minimum elongation ratio at spray angle φ is obtained from $ER(\psi) - ER(\phi)$. The next equation holds:

$$ER(\psi) - ER(\phi) = ER(\varphi - \varepsilon) - ER(\varphi + \varepsilon) \qquad (3)$$

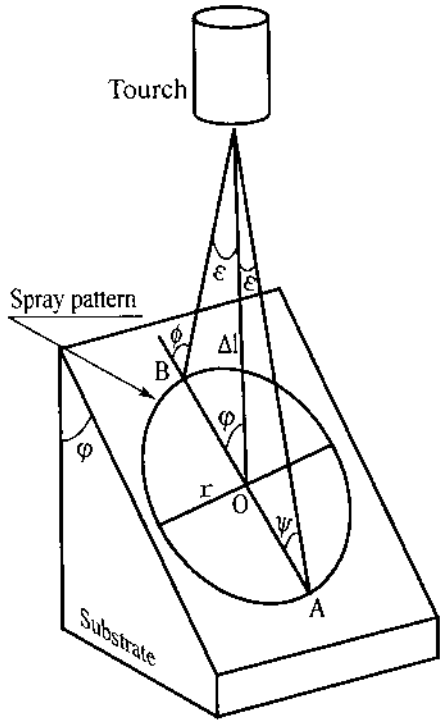

Fig. 13. The broadening powder stream and the variation of impinging angle.

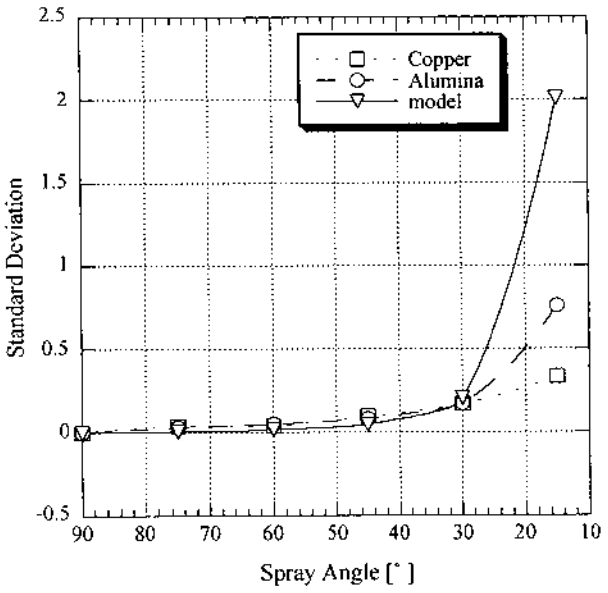

Fig. 14. The comparison of the standard deviation with the variation caused by the broadened particle stream.

because $\phi = \varphi + \varepsilon$ and $\psi = \varphi - \varepsilon$.

The value obtained by substituting $\varepsilon = 1°$ into Eq. 3 and the standard deviation in the case of copper and alumina are shown Fig. 14. The variation of the experimental results appears to be explained by the broadened powder stream from the plasma torch.

Conclusions

The splat shape sprayed at off-normal angle is elliptic. In particular, the profiles of the oxide splats were clear and fit an elliptical-shaped footprint quite well. The metal splat contours also agreed with the elliptic curves except for projections peripheral.

The relationship between the major and minor diameters showed strong linearity over the wide range of splat sizes. This implies that the elongation ratio does not depend on the particle diameter and the impact velocity. This behavior appears to validate the model because the model equation does not contain either the particle diameter or the impact velocity explicitly.

The experimental results of the elongation ratio on all the materials were very similar in the range of 90° to 30°. The results at 15° varied and were dependent on the material.

The model agreed well with the elongation ratio of the experimental results in the range between 90° and 30°. The model values were over-estimated than the practical results at spray angles less than 15°.

References

1. M. F. Smith, R. A. Neiser and R. C. Dykhuizen, An Investigation of the Effects of Droplet Impact Angle In Thermal Spray Deposition, Thermal Spray Industrial Applications, Boston, 20-24 June 1994, 603-608.
2. S. H. Leigh and C. C. Berndt, Evaluation of off-angle thermal spray, Surface and Coatings Technology 89 (1997) 213-224.
3. R. C. Tucker, Jr. and M. O. Price, The Effect of Angle of Deposition on The Properties of Selected Detonation Gun Coatings. Proceedings of ATTAC'88, Osaka, Japan, May 1988, 61-71
4. G. Montavon, C. C. Coddet, S.Sampath, H. Herman and C. C. Berndt, Vacuum Plasma Spray Forming of Astroloy, An Investigation of Processing Parameters, Thermal Spray Industrial Applications, Boston, 20-24 June 1994, 469-475.
5. G. Montavon, S.Sampath, C. C. Berndt, H. Herman and C. C. Coddet, Surface and Coatings Technology 91 (1997) 107-115.
6. G. Montavon and C. C. Coddet, 3-D Profilometries of Vacuum Plasma Sprayed Nickel-Based Alloy Splats Using Scanning Mechanical Microscopy, Advances in Thermal Spray Science & Technology, Houston, Texas, 11-15 September 1995, 285-289.
7. V. V. Sobolev and J. M. Guilemany, Droplet Flattening During Thermal Spray at Off-Normal Angles, Thermal Spray (Meeting the Challenges of the 21st Century), Nice, France, 25-29 May 1998, 497-502.
8. H. Fukanuma, C-J. Li, Mathematical modeling of splat formation at off-normal angles in thermal spray, Proceedings of United Thermal Spray Conference, Düsseldorf, Germany, 17-19 March 1999, 513-518.
9. M. Bussmann, S. Chandra, and J. Mostaghimi, Numerical results of off-angle spray particle impact, Proceedings of United Thermal Spray Conference, Düsseldorf, Germany, 17-19 March 1999, 783-786.
10. J. Madejski, Solidification of Droplets on A Cold Surface, Int. J. Heat Mass Transfer Vol. 19 (1976), 1009-1013.
11. H. Fukanuma and A. Ohmori, Behavior of Molten Droplets Impinging on Flat Surface, Proceedings of the Thermal Spray Industrial Applications, Boston, 20-24 June 1994, 563-568.